Tracer diffusion of oxygen in $Bi_2Sr_2CaCu_2O_x$

M. Runde,* J. L. Routbort, and S. J. Rothman
Materials Science Division, Argonne National Laboratory, Argonne, Illinois 60439

K. C. Goretta
Materials and Components Technology Division, Argonne National Laboratory, Argonne, Illinois 60439

J. N. Mundy and X. Xu
Materials Science Division, Argonne National Laboratory, Argonne, Illinois 60439

J. E. Baker
Center for Microanalysis of Materials, University of Illinois, Urbana, Illinois 61801
(Received 1 October 1991)

Tracer diffusion of ^{18}O has been investigated in dense polycrystals and in the c direction in single crystals of $Bi_2Sr_2CaCu_2O_x$ between 300 and 700 °C under one atmosphere of oxygen. Penetration profiles were determined by secondary-ion mass spectrometry. The diffusional anisotropy as measured by the ratio of the diffusion coefficients in the polycrystals [$D=1.7\times10^{-5}\exp(-0.93\ \text{eV}/kT)\ \text{cm}^2/\text{s}$] to the diffusion coefficients parallel to the c axis of the single crystals [$D=0.6\ \exp(-2.20\ \text{eV}/kT)\ \text{cm}^2/\text{s}$] is large and temperature dependent. The results suggest that diffusion in the ab plane and in the c direction takes place by different mechanisms.

I. INTRODUCTION

The superconducting properties of $Bi_2Sr_2CaCu_2O_x$ (BSCCO) depend on oxygen content:[1–5] The superconducting transition temperature T_c decreases[5] for $x \geq 8.18$ and is dependent on annealing temperatures and cooling rates.[6] Oxygen vacancies have also been suggested as a major source of flux pinning in BSCCO.[7] The kinetics of oxygen motion and the formation and migration of oxygen defects in BSCCO can be studied by measurement of the oxygen-tracer diffusion parameters; these provide not only input to theoretical point-defect models, but can also be useful in developing fabrication techniques.

The pseudotetragonal 85-K BSCCO superconductor $Bi_2Sr_2CaCu_2O_x$, or 2:2:1:2, consists of one Ca atom symmetrically located between the layer sequences Cu-O, Sr-O, and Bi-O, each layer parallel to the ab plane.[6,8] Because the structure is pseudotetragonal, diffusion in BSCCO can be described by two diffusion coefficients, one in the ab plane and one parallel to the c direction. X-ray analysis[9] indicates that the cations and anions in BSCCO undergo incommensurate modulations. These modulations have been attributed to the presence of extra oxygen ions in the Bi-O layer.[10] The presence of the extra oxygen ions in the Bi-O layer suggests that diffusion in the ab plane occurs via an interstitial mechanism. Diffusion in the c direction, on the other hand, involves crossing Sr-O, Cu-O, and Ca planes, on which there are no low-energy sites for oxygen interstitials and on which the concentration of vacant oxygen sites is low. Diffusion in the ab plane could thus be much faster than along the c direction.

Tracer diffusion of oxygen in $YBa_2Cu_3O_{7-\delta}$ (YBCO) single crystals is highly anisotropic, with $D_{ab} \gg D_c$.[11–13] Tracer and internal-friction measurements indicate that oxygen diffusion in the ab plane occurs via a modified interstitial mechanism. The proposed mechanism is that an oxygen ion at the end of a segment of a chain of oxygen ions jumps into a site on the neighboring empty row, moves along the vacant row until it comes to another chain segment end, and attaches itself there.[12] The activation energy for diffusion in the ab plane is 0.97 eV, whereas for the c direction it is ≈ 1.8 eV. (The latter value was calculated assuming that the lowest diffusion coefficient measured at each temperature represents pure c-direction diffusion.) The difference in activation energies suggests that the diffusion mechanisms in the ab plane and c direction may not be the same.

The present paper describes similar measurements of the tracer diffusion of ^{18}O in both poly- and single crystals of $Bi_2Sr_2CaCu_2O_x$ in the temperature range 300–700 °C at 1 atm (10^5 Pa) of oxygen pressure. Oxygen diffusion along the c axis in single crystals is compared with diffusion in dense polycrystals. The diffusion parameters are calculated and discussed in terms of the crystal structure.

II. EXPERIMENTAL TECHNIQUES

A. Sample preparation

The $Bi_2Sr_2CaCu_2O_x$ single crystals were grown by a self-flux technique. Bi_2O_3, $SrCO_3$, $CaCO_3$, and CuO powders in the cation ratio 2:2:1:2 were ground and mixed in a ball mill. The mixture was then heated in air in a Pt crucible to 1000 °C at a rate of 100–150 °C/h. The sample was held at 1000 °C for 2 h and then cooled to

950 °C in about 3 min. The temperature was further decreased to 750 °C at a rate of 1–3 °C/h and finally lowered to room temperature at 50–100 °C/h. The 10–15-mm large single crystals obtained had a laminated structure, as shown in the scanning electron microscope (SEM) image in Fig. 1. The sheets were typically 2–6 μm thick and delaminated very easily, probably along the *ab* planes. The transition temperature of the single crystals was 85 K as measured with a superconducting quantum interference device (SQUID) magnetometer. X-ray powder diffraction did not reveal the presence of phases other than the 2:2:1:2.

The polycrystals were made from the same powders as used to produce single crystals. First, a composition of $Bi_2Sr_{1.7}CaCu_2O_x$, which has been found to yield 2:2:1:2 of excellent phase purity,[14] was synthesized by solid-state reaction. The starting powders were mixed by ball milling for 24 h in polyethylene jars containing methanol and ZrO_2 grinding media. After being milled the powder mixture was pan dried and ground lightly with an agate mortar and pestle. The powder was placed in a shallow Al_2O_3 crucible and heated in air for a total of 72 h at 815–845 °C. The powder was ground twice during this period to improve homogeneity. Only the 2:2:1:2 phase was detected in the powder by x-ray diffraction.

Eight grams of powder were pressed in a 19-mm cylindrical die at a pressure of 35 MPa. The resultant disk was sintered for 6 h in O_2 at 800 °C to provide sufficient strength for handling and then encased in Ag foil covered by a steel jacket. The metallic can surrounding the disk was evacuated and sealed, and the assembly was then hot isostatically pressed for 2 h in an inert atmosphere at 825 °C under a pressure of 100 MPa.[15] X-ray pole figure analysis revealed that the sample was moderately textured, with the *ab* planes preferentially aligned parallel to the face of the disk-shaped sample. The texture could have resulted from a friction-induced nonhydrostatic component of pressure and/or because of the platelike grain structure of BSCCO.

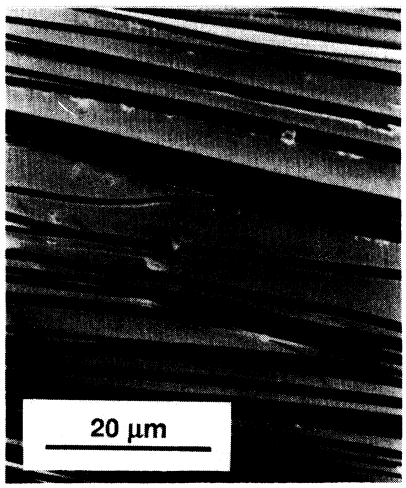

FIG. 1. Secondary-electron micrograph of $Bi_2Sr_2CaCu_2O_x$ single crystal. The bar represents 20 μm.

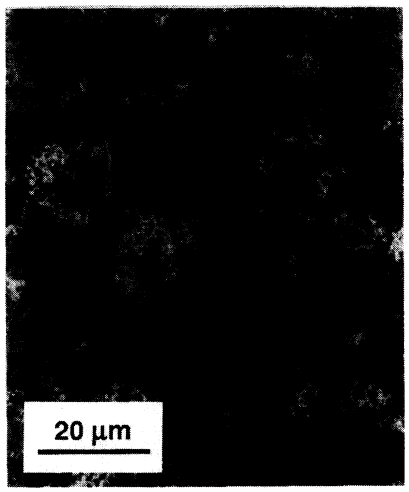

FIG. 2. Secondary-electron micrograph of polished polycrystalline $Bi_2Sr_2CaCu_2O_x$. The bar represents 20 μm.

The resultant polycrystalline BSCCO was more than 95% dense. A SEM micrograph is shown in Fig. 2. X-ray diffraction revealed that the BSCCO consisted of the 2:2:1:2 phase, 5–10 % of the $Bi_2Sr_2CuO_y$ (2:2:0:1) phase (the lighter areas in the micrograph), and residual nonsuperconducting phases. The dark precipitates are CuO. It was difficult to etch the BSCCO and measure the grain size quantitatively. SEM observations on fracture surfaces indicated that the grains consisted of thin, flat plates about 10×10 μm^2 in dimension and about 1 μm thick. The T_c of the as-pressed disk was about 76 K, but was increased to about 85 K by annealing for 16 h in air at 800 °C.

Prior to the experiment, the surfaces of the polycrystalline samples were polished with diamond paste down to 0.25 μm grit. The single crystals were cleaved along the natural delaminating planes to reveal a fresh surface parallel to the *ab* planes. The stoichiometries of the samples were adjusted prior to the diffusion anneal by giving the samples a prediffusion anneal in a quartz tube at the same temperature under natural oxygen at a pressure P_{O_2} of 10^5 Pa at the annealing temperature. The prediffusion anneal was always carried out for a much longer time than the diffusion anneal.

The diffusion anneal was performed in a quartz capsule which was evacuated and backfilled with 95% ^{18}O so that the P_{O_2} during the diffusion anneal was the same as during the prediffusion anneal, i.e., 10^5 Pa, and sealed. Since the stoichiometry was not changed during the diffusion anneals, no chemical diffusion occurred, and a true tracer diffusion coefficient could be measured. Temperatures were measured to ±1 °C.

B. Depth profiling

Secondary-ion mass spectrometry (SIMS) was used as the depth-profiling technique. The SIMS technique has been successfully employed for measurements of oxygen diffusion in a wide variety of ceramic oxides, including

the superconductors $La_{2-x}Sr_xCuO_4$ (Ref. 16) and $YBa_2Cu_3O_{7-\delta}$.[11,12]

Concentration profiles were measured with a Cameca 3*f* SIMS or a Vacuum Generator SIMSLAB. The operating conditions for these two instruments were the following: The Cameca 3*f* SIMS had a beam current of 0.2–0.3 μA 17-keV Cs^+ ions, rastering an area of 250×250 μm^2, of which an area 10 μm in diameter was analyzed. The Vacuum Generator SIMS had a beam current of 5–10 nA 10-keV Ar^+ ions, rastering an area of 45×75 μm^2, of which 15×25 μm^2 was analyzed. Both instruments counted the masses 16, 18, and 63 by negative SIMS.

Depth profiling was carried out in two different modes, depending on the depth of the diffusional penetration.[17] For penetrations of a few micrometers or less, a single crater was sputtered (spot-scan mode). The final crater depths were measured with a profilometer. The increment of depth per channel was assumed to be the crater depth divided by the number of channels; i.e., the sputtering rate was assumed to be uniform. However, in a few cases the craters were too shallow to be easily detected in the optical microscope of the profilometer. These crater depths were estimated from the sputtering time, assuming the same sputtering rate as measured on other craters in the same sample.

Time limitations, interference from the crater sides, and roughening of the crater bottoms precluded using the SIMS spot-scan mode for diffusion zones deeper than about 10 μm. Some of the polycrystal samples had much deeper tracer penetrations, and so a taper section (1°–2°) was ground on these samples after the diffusion anneal, and the penetration profile was recorded by automatically stepping an unrastered SIMS beam along a line parallel to the taper in 25- or 50-μm steps (line-scan mode). The angle of the taper was measured with a profilometer, and the depth corresponding to each of the line-scan channels was taken as the distance along the taper times the sine of the taper angle.

In both SIMS modes the concentration c_{18} of tracer for each channel was determined by

$$c_{18}=\frac{N(^{18}O)-N(BG)}{N(^{16}O)+N(^{18}O)} . \quad (1)$$

Here N refers to the raw counts obtained by the SIMS and N(BG) the background of ^{18}O, usually obtained by averaging the ^{18}O counts over the channels of the profile with the lowest ^{18}O counts.

III. RESULTS

A. Single crystals

Diffusion in the single crystals was measured in the *c* direction for annealing times that yielded 1–10-μm-deep diffusion zones. In perfect single crystals, the tracer concentration would decline to the natural background level within this distance. However, this occurred only in a few of the depth profiles. Usually, the ^{18}O concentration initially decreased as expected, but then leveled off and began increasing well before the natural background level was reached. In most depth profiles the analysis was stopped at this point. When the profiling was carried out further, another peak in the tracer concentration was found. Figure 3 shows such a depth profile (plotted as counts versus channel number) from a single crystal annealed for 216 h at 500 °C. (Irregularities near the surface in the SIMS data are not due to diffusion, but represent equilibration of the surface during sputtering.) The peak in the ^{18}O counts around channel 300 indicates that there is an additional tracer source at the corresponding depth (≈4 μm). The most likely explanation of this unusual penetration plot is that the samples consist of macroscopic layers (see Fig. 1), and there are cracks or other discontinuities between the layers. The penetration of the oxygen tracer from the side surfaces of the sample along these discontinuities proceeds at a much higher rate than the bulk diffusion in the *c* direction. Hence the presence of cracks or other diffusion short circuits perpendicular to the sputtering direction may yield a penetration plot with a peak in the tracer concentration at the depth of the diffusion short circuit. The fact that the tracer peak is almost symmetrical and occurs at a depth corresponding to the thickness of a typical laminated sheet supports this conclusion.

The concentration of tracer c_{18} was fit to the complementary-error-function solution of the diffusion equation for constant surface concentration,

$$c_{18}=c_0\,\mathrm{erfc}\{x/[2(Dt)^{1/2}]\} , \quad (2)$$

by means of commercial software[18] in order to obtain values of the tracer diffusion coefficient D. Here c_0 is the surface concentration, x the depth, and t the diffusion annealing time. The first few channels where the sputtering rates had not reached equilibrium were routinely discarded. Channels were included in the fit as long as the ^{18}O counts stayed higher than twice the background. During

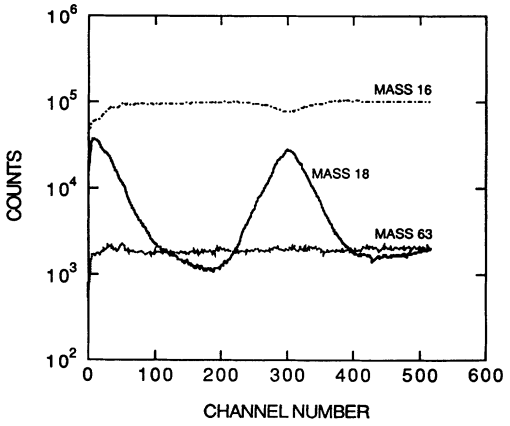

FIG. 3. SIMS spot scan obtained from sputtering along the *c* axis of $Bi_2Sr_2CaCu_2O_x$ single crystal. The counts of ^{16}O, ^{18}O, and ^{63}Cu are shown as a function of channel number (proportional to the penetration distance). The peak in the ^{18}O concentration is caused by tracer penetration along cracks perpendicular to the sputtering direction.

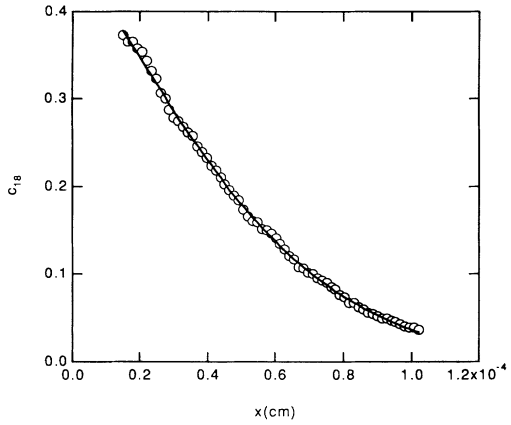

FIG. 4. Penetration plot made from channels 15–75 of the concentration profiles shown in Fig. 3. This single crystal was annealed in ^{18}O at 500 °C for 216 h. The solid line is the least-squares regression fit to Eq. (2).

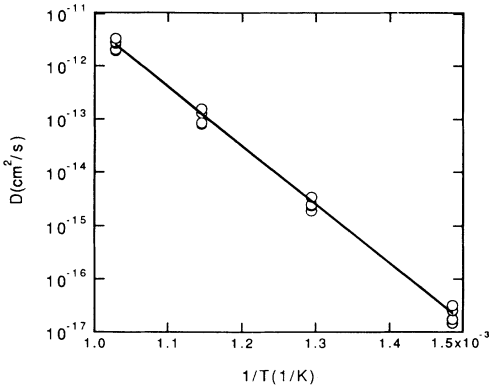

FIG. 6. Arrhenius plot of the diffusion coefficients from oxygen-tracer diffusion in the c direction of single-crystal $Bi_2Sr_2CaCu_2O_x$. The solid line corresponds to a preexponential D_0 of 0.56 cm^2/s and an activation energy Q of 2.20 eV.

fitting, each c_{18} value was assigned a weight equal to the reciprocal of its standard deviation; i.e., it was assumed that the SIMS counts followed zeroth-order Poisson statistics.

Figure 4 shows a penetration plot based on the first part of the depth profiles presented in Fig. 3. The experimental points are shown as circles, and the solution to the diffusion equation [Eq. (2)] is shown as a solid line. Figure 5 shows a penetration plot from another sample that was annealed at 700 °C for 3 h, where the fit to a complementary error function resulted in substantial systematic deviations because the tracer profile has a kink around $x=0.5$ μm. Irregularities similar to this were found in both copper and oxygen profiles from several of the samples, indicating that inhomogeneities were present within the layers, as well as between them. Calculated values of D never changed by more than a factor of 2, and mostly considerably less, if N(BG) in Eq. (1) was taken as the natural background level (2×10^{-3} times the ^{16}O counts), instead of an average over the channels with lowest ^{18}O counts.

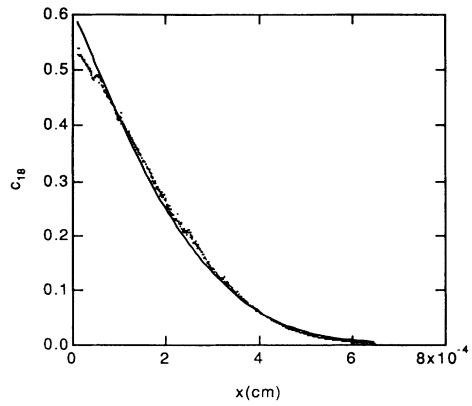

FIG. 5. Penetration plot obtained from a single crystal annealed in ^{18}O at 700 °C for 3 h. The dots show the experimental data, while the solid line is the least-squares regression fit to Eq. (2).

The two penetration plots shown in Figs. 4 and 5 are the best and worst fits obtained from single crystals, as measured by χ^2 and the randomness of the deviations of the experimental data around the least-squares lines. The values of D obtained from 20 penetration plots are given in Table I and plotted in the usual Arrhenius form in Fig. 6. A fit to these data yields

$$D_c=(0.6^{+0.3}_{-0.2})\exp[(-2.20\pm0.03)\ \text{eV}/kT]\ \text{cm}^2/\text{s}\ .$$

These data show considerably less scatter than the earlier measurements on YBCO single crystals[12] where the large anisotropy between diffusion in the ab plane and c direction resulted in a large scatter for diffusion measurements in the c direction because of slight grain misorientations. The better reproducibility in BSCCO compared

TABLE I. Diffusion coefficients for c-axis diffusion in $Bi_2Sr_2CaCu_2O_x$ single crystals.

T(°C)	Time (h)	D (cm^2/s)
400	423	6.12×10^{-17}
400	423	2.48×10^{-17}
400	423	3.11×10^{-17}
400	423	1.68×10^{-17}
400	423	1.42×10^{-17}
500	216	2.49×10^{-15}
500	216	3.38×10^{-15}
500	216	2.36×10^{-15}
500	216	1.85×10^{-15}
500	216	2.04×10^{-15}
600	48	1.55×10^{-13}
600	48	1.33×10^{-13}
600	24	8.07×10^{-14}
600	24	8.28×10^{-14}
700	3	2.72×10^{-12}
700	3	1.85×10^{-12}
700	3	2.66×10^{-12}
700	3	2.52×10^{-12}
700	3	1.95×10^{-12}
700	3	3.14×10^{-12}

with YBCO is the result of having better, larger crystals whose surfaces were cleaved and a smaller difference between c-axis diffusion in single crystals and diffusion in polycrystals (see Sec. III B). Therefore slight misorientations, especially at higher temperatures, would contribute a smaller component of ab diffusion to the measured value of D_c than observed in YBCO.

B. Polycrystals

The analysis of depth profiles from polycrystals must take into account how the SIMS beam averages over the different grain orientations in the sample. Since the analyzed area was of the same order of magnitude as the size of the platelike grains, the beam usually sampled only a few grains.

Penetration plots obtained from the spot-scan measurements can be expected to be the sum of the depth profiles of the individual grains included in the analysis area. Each grain yields a value of D corresponding to the orientation of that grain with respect to the diffusion direction.[11] The spot-scan penetration plots were fitted to an equation of the form

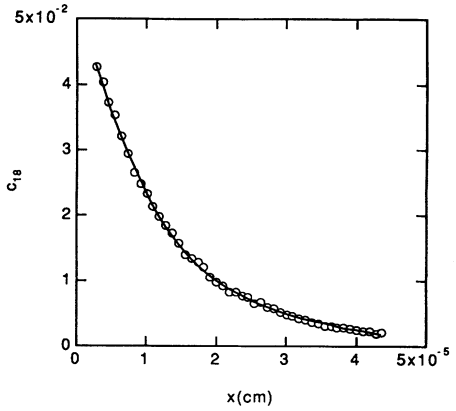

FIG. 7. Penetration plot obtained from polycrystalline $Bi_2Sr_2CaCu_2O_x$ annealed in ^{18}O at 300 °C for 1 h. The solid line is the least-squares fit to Eq. (3).

$$c_{18} = A_1 \operatorname{erfc}\{x/[2(D_1 t)^{1/2}]\} + A_2 \operatorname{erfc}\{x/[2(D_2 t)^{1/2}]\}\ , \quad (3)$$

where D_1 and D_2 are the diffusion coefficients in two

TABLE II. Diffusion coefficients for polycrystalline $Bi_2Sr_2CaCu_2O_x$.

T (°C)	Time (h)	D_1 (cm²/s)	D_2 (cm²/s)	Comments[a,b]
300	1	1.23×10^{-13}	1.13×10^{-14}	SS,PL
300	1	1.16×10^{-13}	1.12×10^{-14}	SS,PL
300	1	5.30×10^{-14}	7.20×10^{-15}	SS,PL
300	1	1.51×10^{-13}	1.03×10^{-14}	SS,PL
300	1	9.16×10^{-14}	1.27×10^{-14}	SS,PL
300	1	1.55×10^{-13}	2.12×10^{-14}	SS,PL
300	6	1.14×10^{-13}	8.86×10^{-15}	SS,PL
300	6	1.29×10^{-13}	6.94×10^{-15}	SS,PL
300	6.25	9.67×10^{-14}	5.39×10^{-15}	SS,PP
300	6.25	9.17×10^{-14}	3.35×10^{-15}	SS,PP
400	2	5.62×10^{-12}	1.53×10^{-12}	SS,PL
400	2	3.49×10^{-12}	[c]	SS,PL
400	2	1.50×10^{-12}	2.59×10^{-13}	SS,PP
400	2	1.14×10^{-12}	2.15×10^{-13}	SS,PP
400	2	1.25×10^{-12}	1.15×10^{-13}	SS,PP
400	2	1.12×10^{-12}	2.81×10^{-13}	SS,PP
500	0.5	2.95×10^{-11}	7.12×10^{-12}	SS,PL
500	0.5	2.81×10^{-11}	1.57×10^{-12}	SS,PL
500	0.5	5.19×10^{-12}	8.26×10^{-13}	SS,PP
500	0.5	6.89×10^{-12}	2.22×10^{-12}	SS,PP
500	0.5	8.36×10^{-12}	4.61×10^{-13}	SS,PP
550	4	1.87×10^{-11}		LS,NA
550	4	2.59×10^{-11}		LS,NA
550	4	2.30×10^{-11}		LS,NA
550	4	2.06×10^{-11}		LS,NA
650	1	2.15×10^{-10}		LS,PP
650	1	2.08×10^{-10}		LS,PP
650	1	2.72×10^{-10}		LS,PP

[a]SS = spot scan and LS = line scan.

[b]Sputtering direction parallel (PL), perpendicular (PP), or unknown (NA) relative to the face of the disk-shaped sample.

[c]A_2/A_1 for this sample was only 10^{-3}, indicating that only one grain was sampled.

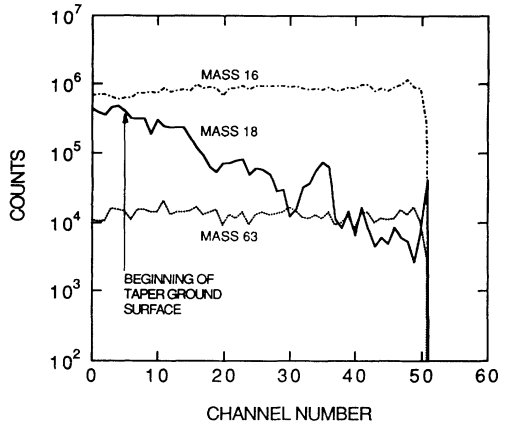

FIG. 8. Line scan obtained from a $Bi_2Sr_2CaCu_2O_x$ polycrystal showing the counts of ^{16}O, ^{18}O, and ^{63}Cu as a function of channel number. The edge of the sample is at channel number 51.

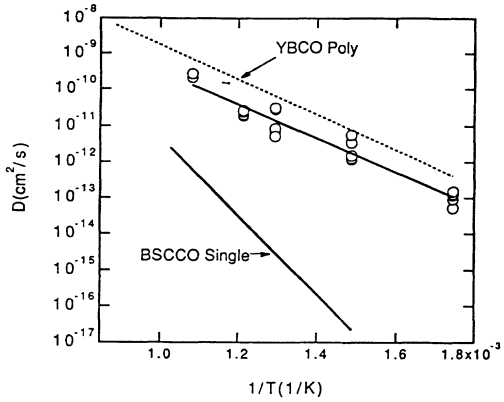

FIG. 10. Arrhenius plot showing the fast-diffusing component D_1 in $Bi_2Sr_2CaCu_2O_x$ polycrystals (circles) and the least-squares fit to these data (the upper solid line). Oxygen-tracer diffusion data from $YBa_2Cu_3O_{7-\delta}$ polycrystals (Ref. 11) (dashed line) and $Bi_2Sr_2CaCu_2O_x$ single crystals results taken from Fig. 6 (lower solid line) are included for comparison.

grains and the constants A_1 and A_2 are proportional to the areas of the two grains. A_1 and A_2 have been assumed to be independent of depth. D_1 is taken as the larger one, implying that the orientation of grain 1 is closer to the faster-diffusion direction than grain 2. (It will be seen later that diffusion in the *ab* plane is much faster than in the *c* direction.) The analysis is limited to two grains to keep the number of parameters within reason. It should be noted that the orientation of the grains can differ from crater to crater and sample to sample, and this adds an unavoidable source of scatter to the data. Smedskjaer[19] has calculated that the standard deviation of a small ensemble of D values can increase as much as 70% as a result of this effect. Figure 7 shows a typical penetration plot obtained from a spot scan of a polycrystal annealed in ^{18}O for 1 h at 300 °C.

In a line scan, each channel represents a different set of grain orientations. Figure 8 shows a line scan on a taper section of a sample annealed at 650 °C for 1 h. A clear indication of anisotropy of diffusion in this type of scan appears as fluctuations in the ^{18}O counts in the diffusion zone that are substantially larger than the fluctuations in the ^{16}O or ^{63}Cu counts. This suggests that these fluctuations are not noise, but are due to anisotropy. The line-scan tracer profile is fit to one complementary error function [Eq. (2)]. Hence this procedure determines an average of D over all the grains hit by the line scan. Figure 9 shows the penetration plot obtained from the line scan of Fig. 8. The solid line represents the least-squares fit, and the circles are the concentration measured every 50 μm along the line scan.

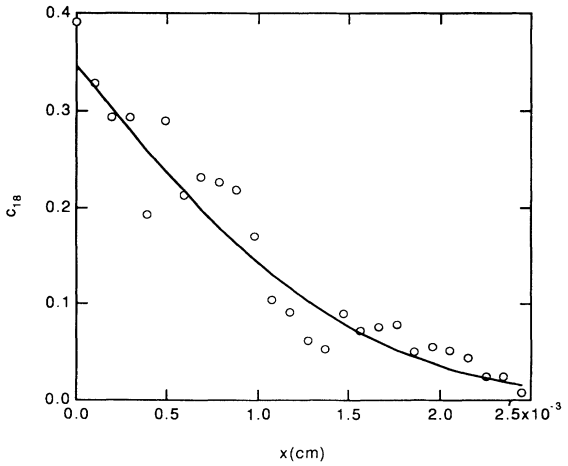

FIG. 9. Penetration plot obtained from the line scan in Fig. 8. This polycrystalline sample was annealed at 650 °C for 1 h. The solid line is the regression fit to Eq. (2).

The diffusion coefficients estimated for both spot- and line-scan measurements on polycrystals are given in Table II. The Arrhenius plot of Fig. 10 includes D values obtained from line scans and the fast-diffusion component (D_1) of the spot-scan measurements. The points fall well on the least-squares line, which is given by

$$D=(1.7^{+1.5}_{-0.8})\times 10^{-5}\exp[(-0.93\pm 0.04)\text{eV}/kT]\ \text{cm}^2/\text{s}\ .$$

As in the case of YBCO, the D_2 values exhibit more scatter than D_1 and are typically one order of magnitude smaller.

The diffusion coefficients in the polycrystals are much larger than D_c obtained from the single crystals. For a tetragonal material, the diffusion coefficient in a grain oriented so that the *c* direction makes an angle θ with the diffusion direction is given by

$$D_\theta = D_{ab}\sin^2\theta + D_c\cos^2\theta\ . \tag{4}$$

The diffusion coefficient in an untextured polycrystal is then obtained by averaging the $\cos^2$ and $\sin^2$ terms over a hemisphere, yielding

$$D_{\text{poly}} = \tfrac{2}{3}D_{ab} + \tfrac{1}{3}D_c\ . \tag{5}$$

D_{ab} cannot be measured on these thin single crystals, but can be estimated from D_{poly} and Eq. (5) because D_c is orders of magnitude less than D_{poly}. In order to bias the

measurements on polycrystals toward D_{ab}, D_1, the larger of the D's in Eq. (3), is taken to represent D_{poly}. Even though the constants in Eq. (5) cannot be evaluated exactly for these samples because of the texture, it can be estimated that the coefficient of the D_{ab} term is $\geq \frac{2}{3}$, and so $D_{\text{poly}} \approx D_{ab}$. The anisotropy of diffusion in BSCCO is thus seen to be very large, but to decrease with increasing temperature.

Because of the large anisotropy, we can approximate the value of the diffusion coefficient for any grain not oriented exactly with the c axis along the diffusion direction by

$$D \approx D_{ab} \sin^2\theta \ . \tag{6}$$

It is the distribution of $\sin^2\theta$ that leads to the scatter due to anisotropy, mentioned above.

Some of the scatter of the data in Fig. 10 and Table II is due to the difference between diffusion experiments performed parallel (PL) and perpendicular (PP) to the face of the disk-shaped samples. The orientations are indicated in Table II. Diffusion perpendicular to the face was slower than diffusion parallel to the face because of the sample texture cited above. Since $D_{ab} > D_c$, D in the PL samples is greater than D in the PP samples because the ab planes are aligned, on the average, more parallel to the surface of the disk. The difference in diffusion coefficients measured in the two directions was up to a factor of 5. No distinction was made to account for orientation in the Arrhenius plot of Fig. 10, because of the scatter due to anisotropy, mentioned above. Nevertheless, the Arrhenius equation for polycrystalline BSCCO fits all of the values of D_1 from the spot scans and D from the line scans within a factor of ± 3.

IV. DISCUSSION

The most interesting result of this investigation is the anisotropy of diffusion. D_c is several orders of magnitude smaller than D_{ab}, and the activation energy Q and preexponential D_0 for diffusion in the c direction are much larger (2.20 eV and 0.6 cm^2/s) than for diffusion in the ab plane (0.93 eV and 1.7×10^{-5} cm^2/s). We believe that this anisotropy is a consequence of different mechanisms being responsible for diffusion in the ab plane and c direction. The presence of an interstitial oxygen atom in the Bi-O planes suggests that diffusion in the ab plane takes place by an interstitial mechanism, and the low value of D_0 supports this idea. The activation energy is low because the interstitial is already there, and no formation energy is needed. Therefore, the activation energy consists of only an energy of motion. On the other hand, the value of D_0 for diffusion in the c direction being of order unity suggests a vacancy mechanism, in analogy with the Zener theory of diffusion in metals.[20] The activation energy in this case is high because both a vacancy formation energy and a vacancy motion energy are required. If this suggestion is correct, the P_{O_2} dependence of D_{ab} and D_c should be of opposite sign; D_c should increase and D_{ab} decrease with decreasing P_{O_2}.

Additional evidence to support the idea that diffusion in the ab plane takes place in the Bi-O planes comes from a preliminary measurement of oxygen diffusion in the ab plane of a $Bi_2Sr_2CuO_y$ (2:2:0:1) single crystal.[21] The value of D at 350 °C is very close to the Arrhenius line for diffusion in 2:2:1:2, which suggests that the environment of the diffusing oxygen atom is the same in 2:2:0:1 as it is in 2:2:1:2. The incommensurate modulation in the Bi-O plane which is caused by the oxygen interstitial in 2:2:1:2 is also present in 2:2:0:1,[9] and the environment of the interstitial is the same. On this basis, one would expect that diffusion in the ab plane of 2:2:0:1 would be the same as diffusion in the ab plane of 2:2:1:2 and would take place in the Bi-O planes. Diffusion in the c direction of 2:2:0:1, on the other hand, might be faster than in the c direction of 2:2:1:2 because the distance between the Bi-O planes is shorter. Therefore the anisotropy of diffusion in the 2:2:0:1 would be less than in 2:2:1:2.

Turner's recent measurements of the mechanical aftereffect[22] on $Bi_{1.8}Pb_{0.4}Sr_{2.0}Ca_{2.2}Cu_3O_y$ yield a relaxation time of 100 s. If a preexponential of the order of the Debye frequency, $10^{13\pm1}$ s^{-1}, is assumed, an activation energy of 0.89 ± 0.06 eV is calculated from these data. Turner's suggestion that this relaxation is due to the motion of oxygen is consistent with the activation energy reported above.

The same planes of defective bonding that we think are responsible for the rapid diffusion parallel to the delamination plane leading to the double peaks in the tracer concentration in the c direction in single crystals (Fig. 3) may also exist in the polycrystals, but we do not believe that diffusion along these planes is responsible for the results obtained from polycrystals. Our reasons are, first, the agreement of the activation energies for the ab-plane diffusion and the mechanical aftereffect, and second, such structures were not observed in the hot isostatically pressed polycrystals by SEM (contrast Figs. 1 and 2), transmission electron microscopy, and SIMS imaging using a 0.2-μm beam.

The results for the tracer diffusion of oxygen in BSCCO and YBCO are quite similar in that the diffusion in both is anisotropic with $D_{ab} \gg D_c$, and the activation energies for diffusion in the ab plane are the same within the experimental uncertainty. In the case of YBCO, we have proposed that diffusion in the ab plane also takes place by an interstitial-type mechanism. However, the structures of the two materials are quite different, the ordered rows of oxygen ions that characterize the structure of YBCO do not exist in BSCCO, and diffusion in the ab plane of the latter material is probably less anisotropic than in YBCO. Further, the calculation of Ronay and Nordlander for oxygen diffusion in YBCO (Ref. 23) suggests that the activation energy for motion in the b direction (i.e., diffusion in the ab plane because of twinning) is close to zero; i.e., the activation energy for diffusion is mostly the energy to form the interstitial, whereas we believe that in BSCCO the activation energy for diffusion is mostly the motion term.

V. SUMMARY

Oxygen diffusion in $Bi_2Sr_2CaCu_2O_x$ is highly anisotropic, with

$$D_{poly} \approx D_{ab} = 1.7 \times 10^{-5} \exp(-0.93 \text{ eV}/kT) \text{ cm}^2/\text{s}$$

and

$$D_c = 0.6 \exp(-2.20 \text{ eV}/kT) \text{ cm}^2/\text{s} .$$

It is suggested that diffusion in the *ab* plane takes place by the motion of the interstitial in the Bi-O planes, whereas diffusion in the *c* direction is by a vacancy mechanism.

ACKNOWLEDGMENTS

The authors are grateful to A. C. Biondo for performing the texture measurements, Dr. C.-Y. Chu for SEM, Dr. D. Miller for transmission electron microscopy, Dr. C. L. Wiley for SIMS analysis, Professor T. Turner for communicating research results before publication, and Dr. L. C. Smedskjaer, and Dr. D. J. Lam for fruitful discussions. This work was supported by the U.S. Department of Energy, BES-Materials Sciences, and by Conservation and Renewable Energy, under Contract Nos. W-31-109-ENG-38 (Argonne) and DE-AC 02-76ER01198 (University of Illinois). One of the authors (M.R.) gratefully acknowledges partial support from the Royal Norwegian Council for Scientific and Industrial Research (NTNF).

*Permanent address: Norwegian Electric Power Research Institute 7034 Trondheim-NTH, Norway.

[1]H. Niu, N. Fukushima, and K. Ando, Jpn. J. Appl. Phys. **27**, L1442 (1988).
[2]D. E. Morris, C. T. Hultgren, A. M. Markelz, J. Y. T. Wei, N. G. Asmar, and J. H. Nickel, Phys. Rev. B **39**, 6612 (1989).
[3]J. Zhao and M. S. Seehra, Physica C **159**, 639 (1989).
[4]M. R. Presland, J. L. Tallon, R. G. Buckley, R. S. Liu, and N. E. Flower, Physica C **176**, 95 (1991).
[5]H.-C. I. Kao, W. L. Chen, T. P. Wei, J. C. Lin, and C. M. Wang, Physica C **177**, 376 (1991).
[6]J. M. Tarascon, W. R. McKinnon, P. Barboux, D. M. Hwang, B. G. Bagley, L. H. Greene, G. W. Hull, Y. LePage, N. Stoffel, and M. Giroud, Phys. Rev. B **38**, 885 (1988).
[7]E. M. Chudnovsky, Phys. Rev. Lett. **65**, 3060 (1990).
[8]R. M. Hazen, C. T. Prewitt, R. J. Angel, N. L. Ross, L. W. Finger, C. G. Hadidiacos, D. R. Veblen, P. J. Heaney, P. H. Hor, R. L. Meng, Y. Y. Sun, Y. Q. Wang, Y. Y. Xue, Z. J. Huang, L. Gao, J. Bechtold, and C. W. Chu, Phys. Rev. Lett. **60**, 1174 (1988).
[9]H. W. Zandbergen, W. A. Groen, F. C. Mijlhoff, G. van Tendeloo, and S. Amelinckx, Physica C **156**, 325 (1988).
[10]V. Petricek, Y. Gao, P. Lee, and P. Coppens, Phys. Rev. B **42**, 387 (1990).
[11]S. J. Rothman, J. L. Routbort, and J. E. Baker, Phys. Rev. B **40**, 8852 (1989).
[12]S. J. Rothman, J. L. Routbort, U. Welp, and J. E. Baker, Phys. Rev. B **44**, 2326 (1991).
[13]S. Tsukui, T. Yamamoto, M. Adachi, Y. Shono, K. Kawabata, N. Fukuoka, S. Nakanishi, A. Yanase, and Y. Yoshioka, Jpn. J. Appl. Phys. **30**, L973 (1991).
[14]F. K. Karbarz, O. D. Lacy, K. C. Goretta, U. Balachandran, D. Shi, J. G. Chen, M. Xu, and M. C. Hash, Mater. Res. Bull. **25**, 251 (1990).
[15]A. S. Nash, P. Nash, H. Shi, R. B. Poeppel, and K. C. Goretta, Supercond. Sci. Technol. **3**, 556 (1990).
[16]J. L. Routbort, S. J. Rothman, B. K. Flandermeyer, L. J. Nowicki, and J. E. Baker, J. Mater. Res. **3**, 116 (1988).
[17]S. J. Rothman, J. L. Routbort, J. E. Baker, L. J. Nowicki, K. C. Goretta, L. J. Thompson, and J. N. Mundy, in *Diffusion Analysis and Applications,* edited by A. D. Romig, Jr. and M. A. Dayananda (The Minerals, Metals and Materials Society, Warrendale, PA, 1989), pp. 289–305.
[18]IGOR, WaveMetrics, Lake Oswego, OR 97035.
[19]L. C. Smedskjaer (private communication).
[20]C. Zener, J. Appl. Phys. **22**, 372 (1951).
[21]M. Runde, J. L. Routbort, J. N. Mundy, S. J. Rothman, C. L. Wiley, and X. Xu (unpublished).
[22]T. J. Turner (private communication).
[23]M. Ronay and P. Nordlander, Physica C **153-155**, 834 (1988).

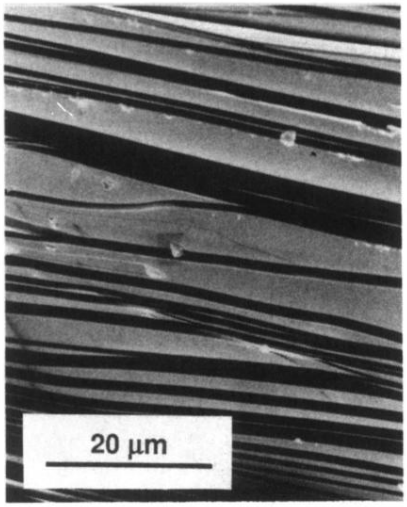

FIG. 1. Secondary-electron micrograph of $Bi_2Sr_2CaCu_2O_x$ single crystal. The bar represents 20 μm.

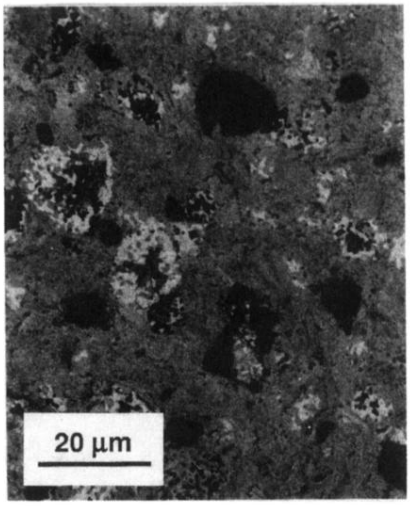

FIG. 2. Secondary-electron micrograph of polished polycrystalline $Bi_2Sr_2CaCu_2O_x$. The bar represents 20 μm.